Strategies to increase austenite FCC relative phase stability in High-Mn steels

L. M. Guerrero[1,2], P. La Roca[1,2,3], M.F. Malamud[1,2], A. Butera [1,2,4], A. Baruj[1,2], M. Sade*[1,2]

[1] Centro Atómico Bariloche (CNEA), Instituto Balseiro (UNCuyo–CNEA), Av. Bustillo 9500, 8400 Bariloche, Argentine

[2] CONICET, Argentine

[3] Institute for Advanced Materials (INAMAT), Universidad Pública de Navarra, Campus de Arrosadia, 31006 Pamplona, Spain

[4] Instituto de Nanociencia y Nanotecnología, CNEA–CONICET

Abstract: Several strategies to increase the FCC austenite stability compared to BCC and HCP martensites have been tested and are discussed. The relative stability of the different phases was analyzed by studying the effects of: a) grain size, b) antiferromagnetic ordering of the austenite, c) thermal cycling through the FCC-HCP transition, d) plastic deformation of the austenite and e) combined effects. As a first step, the effect of decreasing the grain size was analyzed in Fe-Mn alloys for Mn contents smaller than 18 wt.%, where BCC and HCP martensites compete in stability. Formation of the BCC phase is inhibited for 15 wt.% and 17 wt.% of Mn for grain sizes smaller than 2 μm. This enabled, for the first time at these compositions, the measurement of the Néel temperature of the austenite using specific heat and magnetic measurements. A comparison of the obtained transition temperatures with accepted models is discussed. The effect of modifying the grain size on the FCC-HCP transition temperatures was also analyzed for 15 wt.% and 17 wt.% Mn contents showing a complete HCP inhibition for grain sizes smaller than 200 nm. A nucleation model for the HCP martensite is considered which includes an additional resistance to the transformation term depending on the austenitic grain size. Additional combined effects on the FCC stabilization are discussed like the interaction between the antiferromagnetic ordering and the introduction of defects by thermal cycling through the martensitic transformation. The analysis can be easily applied to systems with a larger number of components. Results obtained in the Fe-Mn-Cr system are also presented.

Keywords: FCC-HCP MARTENSITIC TRANSITION, HIGH Mn STEELS, AUSTENITE STABILIZATION, FCC MAGNETIC ORDERING, THERMAL CYCLING

1. Introduction

High Mn steels show several interesting mechanical and functional properties. Most of them are related to the presence of martensitic phase transformations [1, 2]. The composition of the alloy plays the main role concerning the type of phase transition which takes place. The following properties are nice examples of scientific and technological interest: shape memory effect [3-6], pseudoelasticity [7-10], large resistance to low cycling fatigue [11-13], high damping capacity [14,15], good mechanical behavior at cryogenic temperatures [16], large plastic deformation simultaneously with large mechanical stresses [17-23]. Concerning this last effect, large plastic deformations are indeed obtained by the development of martensitic transitions, *i.e.*, the TRIP

(Transformation Induced plasticity) effect, leading to excellent mechanical properties. In fact, recently developed Fe-Mn-Co-Cr alloys display very good mechanical properties related to the TRIP effect, leading to the progress in the field of High Entropy Steels (HESs) [24-26].

The optimization of the mentioned properties requires a precise control of composition. The chemical composition largely determines the type of martensitic phase transition taking place, the martensitic transformation temperatures and the temperature of magnetic ordering of the austenitic structure [2,27,28]. The relevance of the magnetic ordering of the FCC structure has been clearly shown in Fe-Mn based alloys, since this structure is strongly stabilized by the para-antiferromagnetic transition, leading to a strong effect on the martensitic transformation temperatures [27-32].

There is a large amount of studies about the effect of adding elements on the critical martensitic transformation temperatures and on the magnetic ordering temperatures, leading to relevant data for designing new alloys [2,26-34]. However, it is also known that changes in microstructure can be reliable tools in order to have an additional mechanism to control martensitic transformation temperatures. Just as an example, plastic deformation by rolling at 400 °C can inhibit the FCC-HCP transformation in Fe-Mn based alloys [26,31]. In this case, the large amount of dislocations introduced by rolling is enough to avoid the formation of martensite. However, this method may have other consequences for Mn contents smaller than 20 wt.% due to the introduction of the BCC martensite. It is also known that changes in grain size can modify martensitic transformation temperatures. Different examples have been reported in the literature. Just to mention a couple of them, in Fe-Mn alloys, M_S (martensite start temperature) decreases when the grain diameter becomes smaller than 30 µm and nucleation might not occur if the grain size is smaller than 1 µm [35]. In case of Cu-based alloys it was reported that M_S strongly decreases if the grain size becomes smaller than 10 µm and other effects were also reported [36], such as the increase in thermal hysteresis [37] and a reduction in the size of the martensitic plate [38,39].

The development of methods to control the relative phase stability and critical transformation temperatures by microstructural changes has several positive consequences if Fe-Mn based alloys are considered. On the one hand, an additional degree of freedom is added to composition when alloy design is performed. On the other hand, specific advantages appear when technological applications are taken into consideration: a) a decrease in the amount of thermal martensite can be obtained, thus improving the efficiency of shape memory effect, b) if TRIP mechanisms are required, the increase in the amount of austenite enables to get larger deformations when mechanical stresses are applied because deformation is associated to the austenite to martensite transition. Raabe *et al*. have reported an example for FeMnCrCo alloys, where after a reduction of grain size from 45 µm down to 4.7 µm, the amount of austenite strongly increases, decreasing the amount of thermal martensite. In this way, a large ductility was obtained and reported, leading to a strong improvement in the mechanical properties of these alloys [25,40].

It is then very convenient to improve the comprehension of the effects of microstructural variations on the relative phase stabilities, particularly in those cases where mechanical properties are strongly related to martensitic phase transitions. In Fe-Mn-based alloys there are no systematic analysis of the consequences that arise from variations in grain size, specifically in the composition range where both martensitic transitions compete, *i.e.*, FCC-BCC and FCC-HCP. These alloys, which generally contain less than 20 wt.% Mn, are remarkably

significant for technological purposes. An example has been reported for the Fe-Mn-Al-Si system, where it is possible to obtain sequential martensitic transitions (FCC-HCP-BCC) when mechanical stresses are applied. This leads to the simultaneous presence of large deformations and high mechanical stresses [41].

Although alloys with several components are interesting, we initially focus our attention in this manuscript on binary Fe-Mn alloys. Additionally, we have selected the composition range from 12 wt.% up to 18 wt.% Mn. In this composition range, both martensitic structures, BCC and HCP can be thermally and/or stress induced. A decrease in the FCC-HCP martensitic temperatures may increase the effect of the magnetic ordering of the FCC structure on the martensitic transition, due to the strong stabilization of the austenite once it is magnetically ordered. An interesting situation may arise when the critical temperature for the para-antiferromagnetic ordering of the FCC phase is determined by traditional magnetometry techniques. The reason is that a small amount of the ferromagnetic BCC martensite usually masks the signal of the antiferromagnetic phase which is considerably weaker than the ferromagnetic one. Due to this reason, no reported values of the Néel temperature can be found for Mn contents smaller than 18 wt.%. In this manuscript, we present results of this critical magnetic transition temperature obtained by different methods at the mentioned composition range. These measurements have been possible since we have found that the stability of the FCC phase can be extended to lower Mn contents by a decrease of the grain size. In this way the partial or total inhibition of the nucleation of HCP and BCC martensite enables the detection of the magnetic ordering of the austenite. We show here that it is possible to control the grain size of austenite leading to an increase of the stability of the FCC phase, and to a decrease in the amount of martensite, either BCC or HCP. Additionally, precise results for the temperatures of the antiferromagnetic ordering of the austenite have been obtained and are analyzed in the frame of previous results reported for larger amounts of Mn. Finally, several results concerning combined phenomena, *i.e.*, related to microstructural changes and FCC antiferromagnetic ordering are also analyzed. These results can be relatively easily extended to ternary Fe-Mn-X alloys or even to systems with a larger amount of components. An example is also presented and analyzed here for the Fe-Mn-Cr system.

2. Experimental procedure

Fe-Mn and Fe-Mn-Cr alloys were melted in an arc furnace under argon atmosphere. Pure metals (>99.98 %) were used and the compositions of the alloys are shown in Table 1. The as-melted alloys were subjected to a homogenization heat treatment at 1000 °C for 48 hours encapsulated in quartz with Ar, followed by quenching in water at room temperature by breaking the capsule. Samples of different geometry were cut with a spark cutter machine. The compositions were determined with an Oxford X-Max 80 energy dispersive spectrometry (EDS) detector in a SEM Zeiss Crossbeam 340. EDS data were acquired and treated with AZTEC 3.1 software. Table 1 shows that measured composition values are very close to the nominal ones. Samples of 1 mm × 3 mm × 20 mm, were cut from the buttons using a spark cutter. They were later polished, individually encapsulated into quartz tubes under Ar atmosphere, annealed for 1 h at 1000 °C, and water quenched by breaking the capsules. After this thermal treatment samples are called "as cast" samples. In order to decrease the grain size, samples were 70 % cold rolled and subjected to different thermal treatments between 550 °C and 1100 °C during 5 min. More details will be given below where results are described.

Resistivity measurements were obtained by the four-point method with a homemade equipment using a HP34420A nanovoltmeter. X-ray measurements have been performed at room temperature (RT), using a Bruker

D8 Advance X-ray diffractometer. For X-ray measurements, samples were chemically polished with a solution of 90 vol.% H_2O_2 – 5 vol.% HF – 5 vol.% HNO3 for about 40 s in order to eliminate surface damage.

Austenite grain sizes (Gs) were measured using the intercept line method according to the ASTM E1 12-12 standard. For samples with grain sizes higher than 30 µm micrographs were obtained with an optic microscope Leica DMRM with polarized light. For this purpose, the specimens were mechanically polished from 600 until 2000 grit papers. Then, they were polished using a colloidal silica suspension and, to reveal grain boundaries, the samples were in addition chemically polished using Nital 5% during 3 min. For samples with grain sizes smaller than 30 µm the required micrographs were taken with a TEM Phillips CM 200UT with an acceleration voltage of 200 kV, or with a STEM detector in the SEM Zeiss Crossbeam 340. For this purpose, discs of 3 mm of diameter were spark cut form the samples and thinned to 150 µm with a 1000 grit sand paper. After that, they were electrolytically polished in a double-jet Struers TenuPol-5 using a solution of 95 vol.% acetic acid and 5 vol.% perchloric acid at RT.

Table 1. Name of the alloys, nominal and measured compositions. Binary alloys are named using the content of Mn while names of ternary alloys indicate approximate contents of Mn and Cr.

Name	Nominal composition (wt.%)	Mn (wt.%)	Cr (wt.%)
17Mn	Fe-17Mn	17.0±0.2	0
15Mn	Fe-15Mn	15.3±0.2	0
13Mn	Fe-13Mn	12.7±0.1	0
17Mn6Cr	Fe-17Mn-6Cr	17.3±0.2	6.1±0.1
27Mn12Cr	Fe-27Mn-12Cr	27.1±0.2	12.2±0.1

Small discs (3 mm diameter and 1 mm height) were prepared by spark erosion for magnetic measurements. They were chemically polished using a solution 90 vol.% H_2O_2 – 5 vol.% HF – 5 vol.% HNO_3 during 40 s. The saturation magnetization was measured using a vibrating sample magnetometer (VSM) Lakeshore 7300. Additionally, the magnetic susceptibility was determined as a function of temperature enabling the measurement of Néel temperatures of the FCC structure. For these measurements a homemade Faraday magnetic balance with a Bruker 10 inch electromagnet and a Cahn 1000 microbalance was used. A homemade cryostat/oven enabled a 0 °C - 200 °C measurement temperature range.

In order to determine the amount of ferromagnetic BCC (α'), we used as a reference a Fe-Mn alloy (13 wt.% Mn), named 13Mn, previously rolled at room temperature from an initial thickness equal to 3 mm down to 0.7 - 0.8 mm (about 75% of reduction). The saturation magnetization of this sample was considered the value corresponding to a 100 % ferromagnetic phase, a fact corroborated by X-ray diffraction. Using a linear relationship it was possible to obtain the amount of BCC in other samples using the measured values of the saturation magnetization for each composition after several thermomechanical treatments.

Specific heat (C_P) measurements were performed using a DSC TA Q2000 under the modulation mode (MDSC) in the temperature range from -90 °C up to 400 °C. A heating rate equal to 3 °C/min was selected, with a modulation amplitude equal to 0.5 °C and a period of 100 s.

3. Experimental results

3.1 Effect of the grain size on the amount of ferromagnetic BCC martensite in Fe-Mn alloys

As it was mentioned in the introduction, several potential devices based on Fe-Mn-based alloys might require the partial or total inhibition of the BCC martensite formation. The shape memory effect, which is based on the FCC-HCP martensitic transition might profit from the inhibition of BCC nucleation. It is known that in Cu-based shape memory alloys, the decrease of the grain size noticeably affects the nucleation and growth of martensite, increasing the stability of the austenite. Direct consequences of this fact are the shift of critical transformation temperatures to lower temperatures, an increase in the thermal hysteresis and in some cases a complete inhibition of the structural transition is also obtained [36-39]. Systematic research on these possibilities is also required for Fe-Mn-based alloys, particularly in the composition range where both martensitic structures BCC and HCP compete. Thus, three Fe-Mn alloys were selected (with 17, 15 and 13 wt.% Mn respectively) and were thermomechanically treated to analyze the effect of grain size on the FCC-BCC transition. The used treatment, based on the results of Takaki *et al*. [35] is the following and will be named from now on as TT1:

a) Samples were cold rolled from the initial thickness value (between 3 mm and 4 mm) down to 30 % of the initial thickness (70 % of deformation). In order to prevent the formation of cracks, this large deformation was obtained through several steps keeping the deformation not larger than 20 % in each one, and b) cold rolling was followed by a further thermal treatment during 5 min at 650 °C. Samples were finally air cooled.

Fig. 1 shows the magnetization as a function of magnetic field for sample 15Mn in two different conditions: as cast (blue) and after thermomechanical treatment TT1 (red). For the sake of comparison, the black curve shows the corresponding measurement for the sample which has 100 % ferromagnetic BCC (reference sample). From these curves it is observed that the as cast sample shows a relatively large value of saturation magnetization due to a large amount of BCC ferromagnetic phase which indicates that approximately 61 % (in weight) of the sample corresponds to this phase. After the TT1 treatment, the saturation magnetization strongly decreases indicating a reduction of the amount of BCC phase down to 1 % (in weight).

(Please, place Fig. 1 about here)

It is remarkable that for the 15Mn alloy, the TT1 treatment is very efficient concerning the suppression of the BCC martensite. This can be rationalized considering that the TT1 thermomechanical treatment resulted in a grain size decrease from 300 µm (as cast sample) down to approximately 2 µm. An image of the sample morphology obtained by TEM after TT1 treatment is shown in Fig. 2.

(Please, place Fig. 2 about here)

In the micrograph, plates with morphology similar to the HCP martensite can be observed (yellow arrows). The presence of HCP was confirmed by X-ray diffraction as detailed below. It seems that the decrease in grain size affects the formation of BCC more strongly than the HCP structure. More research is required to define this point. However, it is known that the volume change between austenite and HCP martensite is smaller than the volume change between austenite and BCC martensite [42-46]. A larger volume change might lead to a more difficult accommodation of the shape change in small grains.

The same type of analysis was performed with alloys 17Mn and 13Mn. In the 13Mn alloy no significant reduction of BCC amount was detected after grain size reduction. On the other hand, for the alloy 17Mn, decreasing the grain size down to 2 μm leads to a 0.1 % (in weight) of BCC phase. However, in this case the alloy in the as cast condition already had a small amount of BCC, just 3 % in weight. As the 17Mn alloy did show a very small amount of BCC phase in both cases, *i.e.*, as cast and after TT1, we have selected this alloy to analyze the effect of grain size on the relative phase stability between FCC and HCP martensite, which will be presented below. Finally, an interesting point is that after getting a strong decrease in the BCC amount for both alloys, 17Mn and 15Mn, it is possible to get in both cases a large fraction of the material in the FCC structure. This gives an excellent opportunity to carry forward an experimental analysis of magnetic properties of this phase as it will be detailed. The presence of large fractions of FCC austenite after TT1 in 17Mn and 15Mn alloys was verified by X-ray diffraction. Results are shown in Fig.3. The diffraction patterns also confirm: a) the presence of HCP martensite after TT1 in 15Mn alloy as shown above by TEM, b) the very small amount of BCC martensite in the as-cast 17Mn alloy and c) the negligible amount of BCC martensite in 17Mn and 15Mn alloys after the TT1 thermomechanical treatment.

(Please, place Fig. 3 about here)

3.2 The para- to antiferromagnetic ordering transition in FCC austenite in Fe-Mn alloys

As it was mentioned in the Introduction, there are several papers showing the relevance of the antiferromagnetic order in the FCC austenite and discussing the way in which this phase increases its stability once the para- to antiferromagnetic transition has taken place. This is the main reason to determine as precisely as possible the critical transition temperatures for the magnetic ordering transition, *i.e.*, the Néel temperatures as a function of the composition.

Experimental results on the Néel temperatures of the FCC phase for Fe-Mn alloys with Mn contents smaller than 20 wt.% are unavailable in the literature, mainly due to the presence of both martensitic structures but more specifically due to the formation of the BCC ferromagnetic martensite. In our case, it has been possible to strongly increase the amount of FCC austenite in 17Mn and 15Mn alloys after the TT1 thermomechanical treatment. This fact enables the measurement of the Néel temperature for both compositions, leading to new results not obtained up to this moment. An example of this is shown in Fig. 4, where the Néel temperature is

determined for the 17Mn alloy after TT1 treatment by several experimental methods. Fig. 4a shows the measurement of magnetic susceptibility (defined as dM/dH for H=0) vs. temperature for this alloy, and Fig. 4b presents the curve of specific heat vs. temperature for the same alloy. The same criteria as used in Ref. [26], has been used here to determine the T_N temperature. It is remarkable that two factors allow a successful measurement of the magnetic transition temperature: i) a large fraction of the sample shows the FCC structure and ii) the amount of austenite does not change in the temperature range used to experimentally determine the Néel temperature.

(Please, place Fig. 4 about here)

Fig. 5 shows the obtained Néel temperatures for 17Mn and 15Mn alloys after TT1 thermomechanical treatment. For both alloys the Néel temperature was obtained with the two mentioned experimental techniques: measurements of magnetic susceptibility and specific heat as a function of temperature. It can be observed that the results obtained with different techniques, closely agree considering the measurement precision. Additionally, the obtained results can be compared with tendencies which can be obtained from data presented by other authors where experimental results had been determined for Fe-Mn alloys with larger amounts of Mn [47]. Two interesting tendencies correspond to those presented by Huang (blue line) [48] and by Guerrero *et al.* (black line) [31] respectively. The new data do not exactly fit with the mentioned curves although they show a closer agreement with the black curve in the figure. Additionally, it is shown for the sake of comparison a recently obtained curve which includes data for Fe$_{90-X}$-Mn$_X$-Cr$_{10}$ as a function of Mn content (red curve) [31]. It can be observed that the blue curve, extrapolated from data presented by Huang would intersect the red one for 14 wt.% Mn, which is not reasonable, giving support to the model presented by Guerrero *et al.* which shows a better agreement with experimental data for this range of compositions. Moreover, the dependence of T_N vs. Mn content for the ternary alloy is quite similar to the observed one for the model presented by Guerrero *et al.* at the Mn content range where new data has been obtained in the binary alloys.

(Please, place Fig. 5 about here)

3.3. Effect of the grain size on the relative phase stability between FCC and HCP structures

The 17Mn alloy shows a very small amount of BCC martensite even in the as cast condition. It is then reasonable to use it for the analysis of the effect of grain size on the relative phase stability between the FCC austenite and the HCP martensite. As stated above, the grain size was controlled by modifying the thermomechanical treatment, *i.e.*, after cold rolling deforming 70 %, samples were kept at an aging temperature in the range from 550 °C up to 1100 °C, keeping 5 min at the aging time in all cases, and finally water quenched. This

thermomechanical treatment will be named TT2. Table 2 summarizes the performed treatments, the obtained grain sizes and the FCC to HCP critical transformation temperature M_S.

Table 2. Thermomechanical treatments, grain size values and measured M_S (FCC to HCP critical transformation temperature). The as cast treatment corresponds to 60 min at 1000 °C encapsulated in quartz under Ar atmosphere, and quenched in water at room temperature by breaking the capsule. The rest of the thermomechanical treatments correspond to the named TT2 one, where after the same deformation (70%), ageing temperature is varied. CR is used to indicate cold rolling performed in several steps to avoid fracture. All cold rolled samples are finally water quenched.

Treatment	Grain size [μm]	M_S [°C]
1000 °C + quenching (as cast)	141±14	161±5
70 % CR + 1100 °C x 5 min	101±11	160±5
70 % CR + 1000 °C x 5 min	45±5	156±5
70 % CR + 850 °C x 5 min	10±1	144±5
70 % CR + 650 °C x 5 min	1.5±0.2	111±5
70 % CR + 550 °C x 5 min	0.2±0.02	87±5

Fig. 6 shows the effect of changing the aging temperature in the TT2 thermomechanical treatments on electrical resistivity vs. temperature curves for the Mn17 alloy. The as cast sample (just aged at 60 min at 1000 °C under Ar atmosphere and water quenched by breaking the capsule) shows the typical FCC-HCP transformation morphology (black curve), as reported in Refs. [28,29]. However, after thermomechanical treatment TT2 and as the aging temperature decreases, several features can be observed: a) the temperature range involving the FCC-HCP transition increases leading to an increase of the thermal hysteresis ($A_F – M_S$) in the whole cycle, b) the step in electrical resistivity during the FCC-HCP transition decreases which indicates a reduction of the amount of formed martensite leading to a nearly complete suppression of the martensitic transition (red curve) and c) the FCC-HCP transformation temperature M_S decreases (see black narrows). This last fact leads to a correlation between the grain size and the critical transformation temperature M_S.

(Please, place Fig. 6 about here)

Fig. 7 shows the measured M_S values obtained from the electrical resistivity measurements plotted in Fig. 6 vs. the grain sizes obtained for the alloy 17Mn. Additionally, data reported by Takaki *et al*. for a Fe-15Mn alloy are also included in the figure [35]. Both data groups show a similar behavior indicating that grain size plays an important role on M_S. It is remarkable that M_S strongly decreases for grain sizes smaller than 30 μm. For larger grain sizes the typical effect of Mn content on M_S is visible [28,29], *i.e.* the increase of Mn content decreases M_S.

Both Figures, 6 and 7, make it noticeable the strong effect of grain size reduction on the FCC stability, since the martensitic transformation temperatures decrease as well as the fraction of the HCP structure until finally, it does not form anymore. It is then reasonable to assume that both mechanisms, *i.e.*, nucleation and growth of the HCP martensite are affected. Due to this fact, in this manuscript attention will be focused on the effect of grain size on the HCP nucleation, mainly taking into consideration the variations of the critical transformation temperatures, specifically M_S. We will consider the model presented by Olson and Cohen [49] where it is stated that for a critical nucleus size given by an specific number of planes n, the driving force of the transformation $\left(\Delta G_m^{fcc-hcp}\right)$ must be sufficient to overcome the resistance to the transformation which is the sum of the energy barriers which oppose the structural transition. In the original model the reported barriers are the strain energy (E_m^{st}) required to start the martensitic transition and the surface energy (E^{sur}) [49]. The subscript m emphasizes that we are using molar quantities. An energy balance can be presented in the following way:

$$\tau(n) = n\rho\left(\Delta G_m^{fcc-hcp} + E_m^{st}\right) + E^{sur} \qquad \text{Eq. (1)}$$

In the right side of Eq. (1) the difference in Gibbs free energies defined as the Gibbs energy of the HCP phase minus the corresponding one of the FCC, is negative for temperatures lower than T_0, temperature at which both energies are equal. The strain and surface energy terms are positive. The atomic density of the basal plane is named ρ, and given in mol/m^2. The first two terms in the right side of Eq. (1) depend on n, which leads to the concept of critical size of the nucleus. Once the temperature reaches M_S, and specifically for this temperature, both sides are equal to 0 since the absolute value of the driving force equals the resistance to transform, and this occurs for a critical number of n. The reported surface energy is aprox. 14 mJ/m^2 [29,50,51]. Concerning the strain energy, and using precise values of lattice parameters, a value of 42 J/mol was obtained for a binary Fe-Mn alloy with 17 wt.% content [45].

In a recent work by Guerrero *et al.* [52], a method was developed and used to experimentally determine the driving force for the FCC-HCP transformation in Fe-Mn-based alloys. In that manuscript the authors determined that the difference in specific heats between FCC and HCP is negligible in the temperature range limited by M_S and T_0. This leads to the following equation:

$$\Delta G_m^{fcc-hcp}\Big|_T = \frac{\Delta H_m|_{T_0}(T_0 - T)}{T_0} \qquad \text{Eq. (2)}$$

It is clear from Eq. (2) that the driving force as defined in the present work is negative for temperatures lower than T_0. The magnitudes in the right side of Eq. (2) can be experimentally determined. ΔH_m is the difference in molar enthalpy between both phases, and T_0 is obtained as the average between M_S and A_S. [29,53]. The driving force at the start of the transformation can be obtained by making T = M_S in Eq. (2). In this way all the

magnitudes can be replaced by their values in equation 1 and the number of planes required to form the critical nucleus, can be obtained, leading to a value between 4 and 6 for the 17Mn alloy, as reported by other authors [50,52].

It can be observed that the effect of grain size on M_S cannot be explained by Eq. (1), since no term in that equation is related to the grain size. In order to include this effect, we suggest adding a new term acting as a barrier to the transformation. It must be considered that T_0 and the difference in molar enthalpy depend only on composition, and will not be affected by grain size. It is easily observed from Eq. (1) that the driving force depends on M_S, and that a shift of M_S to lower values leads to an increase in the absolute value of the driving force. It is then possible to add a new term E^{Gs}(Gs) which represents the effect of the grain size decrease on the barriers to the transformation. This term is positive and will be compensated by the variation of the driving force as the grain size decreases in the range where M_S is affected. In fact, E^{Gs}(Gs) will increase as M_S decreases. Eq. (3) shows in which way the nucleation model is modified. The superscript used for this term emphasizes its origin and the parenthesis (Gs) remarks that this barrier depends on the grain size.

$$\tau(n) = n\rho\left(\Delta G_m^{fcc-hcp} + E_m^{Gs}(Gs) + E_m^{st}\right) + E^{sur} \qquad \text{Eq. (3)}$$

Eq. (3) is valid for every grain size as the term depending on the grain size should tend to 0 for grain sizes large enough, situation which corresponds to Gs larger than 100 µm in the case of Fe-Mn-based alloys. We introduce just for convenience an M_S value called M_S^∞ for which the additional barrier term related to the grain size, $E_m^{Gs}(Gs)$, equals 0. Following the same guide the driving force corresponding to large grain sizes will be named ΔG_m^∞ and it is the obtained value for the as cast sample. In the same way as in the original model (Eq.1), when the right member reaches the 0 value for a specific grain size, the temperature to accomplish this requirement is the new Ms.

One of the main outputs of the present results is the possibility of obtaining the increase of the required driving forces to start the FCC-HCP transition when the grain size becomes smaller than 100 µm, $\Delta^{Gs}(\Delta G_m)$. With this aim, equations 2 and 3 are combined, leading to Eq. (4). This result requires that the following magnitudes do not vary with grain size: strain energy, surface energy and the critical nucleus size, a reasonable first approximation to the problem.

$$\Delta^{Gs}(\Delta G_m) = \Delta G_m^\infty - \Delta G_m^{Gs} = \frac{-\Delta H_m\left(M_S^\infty - M_S^{Gs}\right)}{T_0} = E_m^{Gs}(Gs) \qquad \text{Eq. (4)}$$

It can be observed that the variation of driving force $\Delta^{Gs}(\Delta G_m)$ is equal to the energy barrier originated in the variation of the grain size, $E_m^{Gs}(Gs)$. However, it is remarkable that through Eq. (4) it is possible to obtain the relationship between the barrier energy and the grain size, using the relationship between grain size and M_S. The result is shown in Fig. 8 where the energy barrier originated in the variation of grain size is plotted vs. Gs. The values of ΔH_m = 2200 J/mol for 17Mn alloy and 2500 J/mol for 15Mn alloys were used [52,53].

A remarkable output of Fig. 8 is that the behavior corresponding to two alloys differing in 2 wt.% Mn content, almost overlap. This indicates that at least in this composition range the additional energy barrier originated in the grain size reduction does not depend on composition and only depends on the grain size. In order to understand the existence of the added energetic barrier to the transformation, it might be useful to compare these results with those obtained in other systems where martensitic transitions take place and similar effects were detected. As an example we can mention the Cu-based alloys where a strong decrease of M_S has been measured as the grain size decreases [36]. As the grain size diminishes, the density of grain boundaries per unit volume increases. As the martensitic transition starts, and martensite tries to grow, grain boundaries do interfere and introduce several difficulties due to elastic and crystallographic incompatibilities. This makes very difficult to accommodate the transformation in reduced volumes and at least three phenomena can be considered to take place:

a) Additional elastic energy is necessary to accommodate the deformations associated to the interaction between the transformation front and grain boundaries,

b) Microplasticity is usually present close to the grain boundaries. This is for example responsible in Cu-based alloys [37] for hysteresis growth and,

c) An increase in surface energy arises since small grains lead to an increase of martensitic plates, reduction of their size and an increase of surface energy density corresponding to martensite-martensite and martensite-austenite interfaces [38].

It is noticed that all mentioned phenomena are combined and affect the energetic barrier which depends on the grain size. Thus, this term also depends on the density of grain boundaries which is proportional to 1/Gs [37]. It is likely that the problem to accommodate the deformation associated to the volume change in small volume regions will increase as the volume change between the involved phases increase. As an example of this, Cu based alloys show an extremely small volume change between austenite and martensite, aprox. 0.2 % [54] while Fe-Mn alloys show a volume change between FCC and HCP martensite close to 2 % and even larger if the FCC to BCC martensite is considered [42,43]. This difference can explain that the 17Mn alloy does not transform anymore if Gs < 200 nm while some Cu based alloys do transform even for Gs < 70 nm [55-57].

3.4 Effect of the plastic deformation of the austenite on its stabilization

As it was mentioned in the Introduction, in several research works on Fe-Mn-based alloys, a thermomechanical treatment was used to completely inhibit the thermally induced martensitic transition. The most typical procedure is to deform at a temperature above M_d (highest temperature at which martensite can be stress induced), for example, 400 °C, a deformation amount close to 50 % [26,31,34]. In this way, magnetic ordering of the austenite could be analyzed in detail without the contribution of martensite formation to different

experimental measurements. As an example, the Néel temperature of the FCC structure was determined in this way.

Two reasons can be used to understand why this method is efficient to inhibit the FCC-HCP martensitic transition. On the one hand it is known that the deformation mechanism depends on the stacking fault energy (SFE) and that this magnitude increases with temperature. Small values of the SFE favor the FCC-HCP transition, while intermediate values lead to twins. Still larger values are related to plasticity through the formation and slip of dislocations [1,58]. It results from all this that at sufficiently large temperatures the martensitic transformation is inhibited and other mechanisms of deformation would take place. The strong increase of dislocation density can shift M_S sufficiently so as to avoid the nucleation of HCP martensite. On the other hand, it is known that the critical stress to induce the martensite increases with temperature according to the Clausius-Clapeyron equation. Concerning this variation, if temperature is sufficiently higher than M_S, normal plastic deformation will determine the mechanical behavior of the material.

It is interesting to consider that when the critical stress to take the material out from the elastic range increases with temperature, it is accepted that the martensitic transition plays a significant role concerning the mechanism of deformation. The dependence of critical transformation stress depends on the entropy change between both phases, and in fact in several systems like Cu-based alloys, entropy changes between austenite and the corresponding martensite, were obtained using the Clausius-Clapeyron equation [59]. In several Fe-Mn-based alloys it has been reported that even in cases where the positive slope is reported, normal plastic deformation might also be involved [7], which might complicate the measurement of entropy change in this way. However, there is no doubt that the sign and value of the entropy change significantly contributes to an increase of the critical stress to induce the FCC-HCP transformation, favoring the plastic deformation for temperatures sufficiently far from M_S.

Finally, it is noticed that this strategy is rather simple and efficient to stabilize the FCC austenite in many Fe-Mn and Fe-Mn-based systems. However, in the present manuscript, for Fe-Mn alloys with Mn contents smaller than 18 wt.%, the introduction of BCC martensite during deformation a T > M_d did not enable using this method for the stabilization of the austenite. Due to this reason, for these compositions the reduction of grain size was considered as the most convenient procedure to stabilize the austenite as discussed in Sections 3.1 and 3.3.

3.5 Effect of combined phenomena on the relative phase stability between FCC and HCP: Thermal cycling through the martensitic transition and magnetic ordering of the austenite.

As mentioned above the volume change associated to the FCC-HCP martensitic transition in Fe-Mn alloys is close to 2 %, which is far above the maximum allowed elastic deformation. A consequence of this is that during the thermally induced martensitic transition microplasticity takes place and dislocations are introduced [60]. These dislocations make the structural transition more difficult leading to a decrease of M_S and an increase of A_S. The amount of these variations between two consecutive cycles decrease with the number of cycles and finally an asymptotic state is reached. As an example, Fig. 9 shows the electrical resistivity vs. temperature curves for sample 17Mn6Cr where the first cycle is plotted in black and the asymptotic cycle 6 is the red curve. Additionally, it is also shown the curve obtained after the thermomechanical treatment which inhibits the

martensitic transformation (70 % deformation rolling at 400 °C) enabling the measurement of the Néel temperature of the austenite which for this composition is 41 °C.

(Please, place Fig. 9 about here)

It is noticed that in this case M_S is always larger than T_N, leading to a final asymptotic value of M_S which is still larger than T_N. Recently it was reported that the asymptotic state after thermal cycling in Fe-Mn-Cr alloys is reached for a smaller number of cycles in those alloys where the volume change between FCC and HCP phases is also smaller if compared with those cases where the volume change increases [61].This seems to be reasonable since large volume changes require more dislocations to accommodate deformation in each cycle making it more complicated to reach a final asymptotic state. In the same work, the authors obtained the energetic barrier originated in the thermal cycling through the martensitic transition as a function of the number of cycles. They also verified that larger volume changes correspond to higher energy barriers to the transformation.

It should also be noticed that in the results shown in Fig. 9 and additional ones presented by Guerrero *et al*. [61], shifts of M_S in Fe-Mn-Cr alloys due to thermal cycling are not larger than 50 °C. However, an interesting phenomenon takes place when an additional mechanism of stabilization like the para-antiferromagnetic ordering of FCC takes place in a combined way. This is a remarkable result and an example is shown in Fig. 10. In the case shown in this figure, electrical resistivity vs. temperature curves for sample 27Mn12Cr are presented. The Néel temperature is higher than M_S corresponding to the first thermal cycling and of course also higher than the shifted M_S values due to thermal cycling. An additional strong effect is detected here since during the 7th cooling experiment (red curve) the FCC to HCP transition is not detected anymore, *i.e.*, the FCC austenite is completely inhibited here and no hysteresis is observed after a complete thermal cycle is performed. Moreover, the Néel temperature can be easily detected here since no martensitic transition takes place either by cooling or heating.

(Please, place Fig. 10 about here)

Fig. 11 shows the variation of M_S with the number of thermal cycles for samples 17Mn6Cr and 27Mn12Cr where the phenomenon just described can be easily noticed. In sample 17Mn6Cr, $T_N < M_S$ the samples reach their asymptotic state after 6 thermal cycles being the total shift of M_S equal to 15 °C. However, in sample 27Mn12Cr, for which $T_N > M_S$, the asymptotic stage is not reached and M_S strongly decreases leading to the complete inhibition of the HCP formation, *i.e.*, complete stability of the FCC structure.

It is worth mentioning that the combined phenomena just described when $T_N > M_S$ originate in two different reasons: a) thermal cycling introduces dislocations mainly due to the volume change between FCC and HCP structures. This increases the resistance to the transformation and the corresponding increase in the energy barrier can be estimated like it was reported by Guerrero *et al*. [61] for Fe-Mn-Cr alloys; b) The para-antiferromagnetic transition in FCC stabilizes this structure since the effect of this magnetic ordering on the Gibbs free energy of the phase does not enable the increase in driving force required for the structural transition to take place [28,29]. Two extreme cases were shown here. However, these combined phenomena can also take place if T_N is smaller than any of the M_S values reached by thermal cycling. This fact increases the potential use of this strategy to stabilize the FCC structure.

(Please, place Fig. 11 about here)

4. Conclusions

In this manuscript several strategies to stabilize the FCC austenite were presented and analyzed. For this purpose, several phenomena affecting both possible martensites, BCC and HCP have been considered. Very satisfactory results have been obtained.

1. In binary 17Mn and 15Mn alloys the reduction of grain size of the austenite to values close to 2 μm enabled the suppression of the BCC martensite.

2. The Néel temperatures of the FCC austenitic structure were measured in binary alloys for compositions where previously the BCC martensite had not enabled obtaining these results. The measured magnetic transition temperatures show some discrepancies with models presented in the literature, fact which opens new and interesting questions to solve.

3. The effect of grain size on the FCC-HCP transition was analyzed using a modified nucleation model that includes an energetic barrier to the transformation. This barrier could be obtained as a function of the grain size.

4. It was shown the way in which combined phenomena like thermal cycling and magnetic ordering can be used to stabilize the austenite with very satisfactory outputs.

5. The different strategies used to alter the relative phase stabilities in Fe-Mn and Fe-Mn-Cr alloys may be used in Fe-Mn based alloys with different additional elements, and constitute useful tools to design new alloys.

5. Acknowledgments

6. References

[1] P. Chowdhury, D. Canadinc, H. Sehitoglu, On deformation behavior of Fe-Mn based structural alloys, Materials Science and Engineering R 122 (2017) 1-28.

[2] P. La Roca, A. Baruj, M. Sade, Shape-memory effect and pseudoelasticity in Fe-Mn-Based alloys, Shap. Mem. Superelasticity (2017) 3:37-48.

[3] H. Peng, J. Chen, Y. Wang and Y. Wen, Key factor achieving large recovery strains in policrystalline Fe-Mn-Si-based shape memory alloys: A review, Adv. Eng. Mater. 2017, 1700741.

[4] Y.H. Wen, H.B. Peng, D. Raabe, I. Gutierrez-Urrutia, J. Chen and Y.Y. Du, Large recovery strain in Fe-Mn-Si-based shape memory steels obtained by engineering annealing twin boundaries, Nat. Commun. (2014) 5, 4964.

[5] A. Druker, P. Vermaut, J. Malarría, The shape recovery conditions for Fe-Mn-Si alloys: An interplay between martensitic transformation and plasticity, Materials Characterization 139 (2018) 319-327

[6] A. Druker, P. La Roca, P. Vermaut, P. Ochin, J. Malarría, Microstructure and shape memory properties of Fe-15Mn-5Si-9Cr-5Ni melt spun ribbons, Materials Science and Engineering A vol. 556 October 30, 2012. p. 936-945.

[7] A. Baruj, G. Bertolino, H.E. Troiani, Temperature dependence of critical stress and pseudoelasticity in Fe-Mn-Si-Cr pre-rolled alloy, Journal of Alloys and Compounds 502 (2010) 54-58.

[8] T. Omori, K. Ando, M. Okano, X. Xu, Y. Tanaka, I. Ohnuma, R. Kainuma, K. Ishida, Superelastic effect in polycrystalline ferrous alloys, Science 333 (2011) 68–71.

[9] P. La Roca, J. Medina, C.E. Sobrero, M, J.A. Malarria, A. Baruj, M. Sade, Effects of B2 nanoprecipitates on the phase stability and pseudoelastic behavior of Fe-Mn-Al-Ni shape memory alloys. MATEC Web of Conferences 33, 04005 (2015).

[10] P. La Roca, A. Baruj, C.E. Sobrero, J.A. Malarria, M. Sade, Nanoprecipitation effects on phase stability of Fe-Mn-Al-Ni alloys. Journal of alloys and compounds, Vol. 708, (2017), Pages 422-427.

[11] I. Nikulin, T. Sawaguchi, K. Tsuzaki, Mater. Sci. Eng. A 587 (2013) 192. Effect of alloying composition on low-cycle fatigue properties and microstructure of Fe-30Mn-(6x)Si-xAl TRIP/TWIP alloys.

[12] J. Millán, S. Sandlobes, A. Al-Zubi, T. Hickel, P. Choi, J. Neugebauer, D. Ponge, D. Raabe, Acta Materialia 76 (2014) 94–105.

[13] T. Sawaguchi, I. Nikulin, K. Ogawa, K. Sekido, S. Takamori, T. Maruyama, Y. Chiba, A. Kushibe, Y. Inouec, K. Tsuzaki, Scripta Materialia 99 (2015) 49–52.

[14] J.H. Jun, D.K. Kong, C.S. Choi, THE INFLUENCE OF Co ON DAMPING CAPACITY OF Fe–Mn–Co ALLOYS. Materials Research Bulletin, Vol. 33, No. 10, pp. 1419–1425, 1998.

[15] Z. Wang, W. Lu, D. Raabe, Z. Li, On the mechanism of extraordinary strain hardening in an interstitial high-entropy alloy under cryogenic conditions, Journal of Alloys and Compounds 781 (2019) 734-743.

[16] A. Nyilas, K. Weiss, G. Grikurov, N. Zoidze, Tensile, fracture, and fatigue crack growth rate behavior of high manganese steels. AIP Conf Proc 824 I (2006) 130-137.

[17] K. Sato, M. Ichinose, Y. Hirotsu, Y. Inoue, Effects of deformation induced phase transformation and twinning on the mechanical properties of austenitic Fe- Mn-Al alloys, ISIJ Int. 29 (10) (1989) 868-877.

[18] T. Sawaguchi, L.-G. Bujoreanu, T. Kikuchi, K. Ogawa, M. Koyama, M. Murakami, Mechanism of reversible transformation-induced plasticity of Fe-Mn-Si shape memory alloys, Scripta Mater. 59 (2008) 826.

[19] E.D. Palma- Elvira, P. Garnica-Gonzalez, J.S. Pacheco-Cedeño, J.J. Cruz Rivera, M. Ramos-Azpeitia, C.G. Garay-Reyes, J.L. Hernández-Rivera, Microstructural development and mechanical properties during hot rolling and annealing of an automotive steel combining TRIP/TWIP effects. Journal of Alloys and Compounds 798, 2019, Pages 45-52.

[20] K. Pranke, M. Wendler, A. Weidner, S. Guk, A. Weiß, R. Kawalla, Formability of strong metastable Fe-15Cr-3Mn-3Ni-0.2C-0.1N austenitic TRIP/(TWIP) steel - A comparison of different base materials. Journal of Alloys and Compounds, 648, 2015, 783-793.

[21] Z. Li, K.G. Pradeep, Y. Deng, D. Raabe, C.C. Tasan, Metastable high-entropy dual-phase alloys overcome the strength-ductility trade-off. Nature 534 (2016) 227.

[22] Z. Wang, W. Lu, D. Raabe, Z. Li, On the mechanism of extraordinary strain hardening in an interstitial high-entropy alloy under cryogenic conditions, J. Alloys Compd. 781 (2019) 734–743. doi:10.1016/j.jallcom.2018.12.061

[23] F. Kies, P. Köhnen, M.B. Wilms, F. Brasche, K.G. Pradeep, A. Schwedt, S. Richter, A. Weisheit, J.H. Schleifenbaum, C. Haase, Design of high-manganese steels for additive manufacturing applications with energy-absorption functionality, Mater. Des. 160 (2018) 1250-1264.

[24] D. Raabe, C. Tasan, H. Springer, M. Bausch, From High-Entropy Alloys to High-Entropy Steels, Steel Research Int. 86 (2015), No. 10, 1127-1138.

[25] Z. Li, K.G. Pradeep, D. Raabe, Metastable high-entropy dual-phase alloys overcome the strength-ductility trade-of, Nature 354 (2016).

[26] M.D. Acciarri, P. La Roca, L.M. Guerrero, A. Baruj, J. Curiale, M. Sade, Effect of FCC anti-ferromagnetic ordering on the stability of phases in Fe60-XMn30Cr10CoX high entropy alloys, Journal of Alloys and Compounds 823 (2020) 153845.

[27] S. Cotes, M. Sade and A, Fernández Guillermet - Fcc/hcp Martensitic Transformation in the Fe-Mn System: Experimental Study and Thermodynamic Analysis of Phase Stabilities. Met. Trans. A., Volume 26A, August 1995, pp. 1957-1969.

[28] S. Cotes, A. Baruj, M. Sade, A. Fernandez Guillermet, Thermodynamics of the g/ε martensitic transformation in Fe-Mn alloys: modelling of the driving force, and calculation of the Ms and as temperatures, J. de Physique, Colloq. C2 5 (1995). C2-83-88.

[29] S. Cotes, A. Fernandez Guillermet, M. Sade, Phase Stability and fcc/hcp martensitic transformation in Fe-Mn-Si alloys: Part II. Thermodynamic Modelling of the Driving Forces and the Ms and as temperatures, J. Alloys Compd. 280 (1998) 168-177.

[30] A. Baruj, S. Cotes, M. Sade, A. Fernández Guillermet, Coupling binary and ternary information in assessing the fcc/hcp relative phase stability and martensitic transformation in Fe-Mn-Co and Fe-Mn-Si alloys, J. Phys. IV France 5 (1995) (C8-373-378).

[31] L.M. Guerrero, P. La Roca, F. Malamud, A. Baruj, M. Sade, Composition effects on the fcc-hcp martensitic transformation and on the magnetic ordering of the fcc structure in Fe-Mn-Cr alloys, Mater. Des. 116 (2017) 127–135. doi:10.1016/j.matdes.2016.12.003

[32] S. Reeh, M. Kasprzak, C.D. Klusmann, F. Stalf, D. Music, M. Ekholm, I.A. Abrikosov, J.M. Schneider, Elastic properties of fcc Fe–Mn–X (X= Cr, Co, Ni, Cu) alloys studied by the combinatorial thin film approach and ab initio calculations, J. Phys. Condens. Matter 25 (2013), 245401. https://doi.org/10.1088/0953-8984/25/24/245401

[33] P. La Roca, P. Marinelli, A. Baruj, M. Sade, A. Fernández Guillermet, Composition dependence of the Néel temperature and the entropy of the magnetic transition in the fcc phase of Fe-Mn and Fe-Mn-Co alloys, Journal of Alloys and Compounds 688 (2016) 594-598.

[34] P. La Roca, L.M. Guerrero, J. A. Kortsarz, A. Baruj, M. Sade, A. Fernandez Guillermet, Anomalous effect of Si additions upon the paramagnetic-to antiferromagnetic transition entropy in fcc high-Mn steels. Journal of Alloys and Compounds 830 (2020) 154554.

[35] S. Takaki, H. Nakatsu, Y. Tokunaga, Effects of austenite grain size on martensitic transformation in Fe15mass%Mn alloys, Materials Transactions, JIM, Vol. 34, No. 6 (1993), pp 489-495.

[36] P.M. La Roca, L.M. Isola, C.E. Sobrero, Ph. Vermaut, J. Malarría, Grain size effect on thermal-induced martensitic transformation of polycrystalline Cu-based shape memory alloys, Materials Today: Proceedings, 2015, pp. S743-S746.

[37] P. La Roca, L. Isola, J. Malarría, Ph. Vermaut, Relationship between grain size and thermal hysteresis of martensitic transformations in Cu-based shape memory alloys. Scripta Materialia 135 (2017) 5-9.

[38] P. La Roca, L. Isola, Ph. Vermaut, J. Malarria, Relationship between martensitic plate size and austenitic grain size in martensitic transformations, Applied Physics Letters 106, 221903 (2015); doi: 10.1063/1.4922195

[39] P. La Roca, L. Isola, Ph. Vermaut, J. Malarría, β-grain size effect on the 18R-martensite microstructure in Cu-based SMA, Procedia Materials Science 8 (2015) 1133 – 1139.

[40] Z. Li, C. Tasan, K. G. Pradeep, D. Raabe, A TRIP-assisted dual-phase high-entropy alloy: Grain size and phase fraction effects on deformation behavior, Acta Materialia 131 (2017) 323-335.

[41] M. Raposo, M. Martín, M.F. Giordana, V. Fuster, J. Malarría, Effects of strain rate on the TRIP-TWIP transition of an austenitic Fe-18Mn-2Si-2Al steel, Metall. Mater. Trans. 50 (2019) 4058-4066.

[42] P. Marinelli, M. Sade, A. Baruj, A.F. Guillermet, Lattice parameters of metastable structures in quenched Fe-Mn alloys. Pt. I. Experimental techniques, bcc and fcc phases, Z. Metallkd. 91 (2000) 957–962.

[43] P. Marinelli, A. Baruj, A.F. Guillermet, M. Sade, Lattice parameters of metastable structures in quenched Fe-Mn alloys. Part II: hcp phase, Z. Met. 92 (2001) 489–493.

[44] P. Marinelli, M. Sade, A. Fernández Guillermet, On the structural changes accompanying the fcc/hcp martensitic transformation in Fe–Mn–Co alloys, Scr. Mater. 46 (2002) 805–810, https://doi.org/10.1016/S1359-6462(02)00080-5.

[45] F. Malamud, L.M. Guerrero, P. La Roca, M. Sade, A. Baruj, Role of Mn and Cr on structural parameters and strain energy during FCC-HCP martensitic transformation in Fe-Mn-Cr shape memory alloys, Materials and Design 139 (2018) 314-323. https://doi.org/10.1016/j.matdes.2017.11.017

[46] F. Malamud, F. Castro, L.M. Guerrero, P. La Roca, M. Sade, and A. Baruj, High-precision face-centered cubic-heagonal close-packed volume-change determination in high-Mn steels by X-ray diffraction data refinements, J. Appl. Cryst. (2020) 53, 34-44.

[47] O.A. Khomenko, I.F. Khil'kevich, G.Y. Zvigintseva, Influence of a third component on the Néel point of iron-manganese invars, Fiz. Met. Metalloved. 37 (1974) 1325–1326.

[48] W. Huang, An assessment of the Fe-Mn system, Calphad 13 (1989) 243–252.

[49] G. B. Olson and Morris Cohen. A General Mechanism of Martensitic Nucleation Part I. General Concepts and the FCC→ HCP Transformation. Metallurgical Transactions A. Vol. 7A, DECEMBER (1976) 1897-1904.

[50] S.T. Pisarik, D.C.V. Aken, Thermodynamic driving force of the g / ε transformation and resulting Ms temperature in high-Mn steels, Metall. Mater. Trans. A 47 (2016) 1009-1018.

[51] J. Nakano, P.J. Jacques, Effects of the thermodynamic parameters of the hcp phase on the stacking fault energy calculations in the Fe-Mn and Fe-Mn-C systems, Calphad Comput. Coupling Phase Diagrams Thermochem. 34 (2010) 167-175.

[52] L.M. Guerrero, P. La Roca, F. Malamud, A. Baruj, M. Sade, Experimental determination of the driving force of the fcc-hcp martensitic transformation and the stacking fault energy in high-Mn Fe-Mn-Cr steels, Journal of Alloys and Compounds, Vol. 797 (2019) 237-245. https://doi.org/10.1016/j.jallcom.2019.05.109

[53] P. Marinelli, A. Baruj, J. Pons, M. Sade, A. Fernandez Guillermet, E. Cesari, The enthalpy change of the hcp-fcc martensitic transformation in Fe-Mn alloys: composition dependence and effects of thermal cycling, Mater. Sci. Eng. A A335 (2002) 137-146.

[54] A. Caneiro, M. Chandrasekaran, Thermoelastic martensitic transformation in β Cu-Zn-Al studied by density changes, Scripta Metelurgica, Volume 22, Issue 11, 1988, Pages 1797-1800.

[55] M.J. Morán, A.M. Condó, F. Soldera, M. Sirena, Martensitic transformation in freestanding and supported Cu–Al–Ni thin films obtained at low deposition temperatures, Materials Letters, 184, 177-180, (2016).

[56] M.J. Morán, A.M. Condo, N. Haberkorn, Recrystallization and martensitic transformation in nanometric grain size Cu-Al-Ni thin films grown by DC sputtering at room temperature, Materials Characterization, 139, 446-451, (2018).

[57] M. Morán, A.M. Condó, S. Bengio, F. Soldera, M. Sirena, N. Haberkorn, Martensitic transformation in free-standing Cu-Al-Ni thin films with micrometric grain size, Materials Research Express 6 (9), 096556, (2019).

[58] P. Chowdhury, H. Sehitoglu, Deformation physics of shape memory alloys - Fundamentals at atomistic frontier, Progress in Materials Science 88 (2017) 49-88.

[59] F. de Castro Bubani, M. Sade, V.Torra, F.Lovey, A.Yawny, Stress induced martensitic transformations and phases stability in Cu–Al–Be shape-memory single crystals, Materials Science and Engineering: A, 583, 2013, 129-139.

[60] A. Baruj, A. Fernández Guillermet, M. Sade, Effects of thermal cycling and plastic deformation upon the Gibbs energy barriers to martensitic transformation in Fe-Mn and Fe-Mn-Co alloys. Materials Science and Engineering A 273-275(1999) 507-511.

[61]   L.M. Guerrero, P. La Roca, F. Malamud, A. Baruj, M. Sade, A short review on the effect of Cr on the fcc-hcp phase transition in Fe-Mn-based alloys, Shape Memory and Superelasticity (2020).https://doi.org/10.1007/s40830-020-00285-z

Figure captions:

Figure 1: Magnetization vs. magnetic field for the sample 15Mn. The blue and red curves correspond to the as cast condition and to the thermomechanically treated sample respectively (TT1). The black curve corresponds to the reference sample which is 100 % in the BCC ferromagnetic state.

Figure 2: Bright field TEM image of sample 15Mn after TT1 thermomechanical treatment. Grain boundaries are easily noticed. Plates with HCP martensite morphology are also observed (yellow arrows)

Figure 3: X-ray diffraction patterns for as cast samples and after thermomechanical treatment TT1. a) Alloy 15Mn and b) Alloy 17Mn.

Figure 4. Measurement of the Néel temperature T_N for 17Mn alloy after TT1 thermomechanical treatment: a) Magnetic susceptibility (arbitrary units) vs. temperature (black), b) Specific heat vs. temperature (blue)

Figure 5: Néel temperatures of the FCC austenite as a function of Mn content for binary Fe-Mn alloys. Data obtained by two different experimental techniques used in this manuscript are included and compared with expected values reported in the literature according to different models [31,47,48]. Experimental data obtained for a ternary alloy [31] are also included, as well as the model describing that behavior.

Figure 6. Electrical resistivity vs temperature for 17Mn alloy. The black curve was obtained for the as cast sample and can be used as a reference example for large grain sizes. The rest of the curves correspond to samples deformed 70 % by cold rolling and aged 5 minutes at different temperatures (TT2 thermomechanical treatment). The aging temperature and corresponding grain size are shown in the inset. The vertical black dashed line indicates the Néel temperature of the alloy. For a few transformation curves, small black and red arrows show the M_S and A_F values respectively.

Figure 7: Variation of M_S with grain size for the 17Mn alloy (this manuscript) and for and Fe-Mn alloy with 15 wt.% reported in Ref. [35].

Figure 8. Energy barrier E_m^{Gs} vs. grain size. Notice that according to Eq. (4), E_m^{Gs} equals the variation of driving force when M_S is shifted from M_S^∞ to the M_S corresponding to grain size.

Figure 9. Electrical resistivity curves vs. temperature for sample 17Mn6Cr for the first cycle (black and for cycle 6 (red curve) which corresponds to the asymptotic state. The blue curve corresponds to the same sample after 70 % rolling deformation at 400 °C. The magnetic transition of the FCC structure is easily observed here.

Figure 10. Electrical resistivity vs. temperature curves for sample 27Mn12Cr. Cycles 1 (black curve) and 7 (red curve) are shown. No martensitic transformation is detected in thermal cycle 7, where the Néel temperature can be easily determined.

Figure 11. Variation of M_S as a function of the number of thermal cycles for samples 17Mn6Cr (blue symbols) and 27Mn12Cr (red symbols). Néel temperatures (T_N) for both alloys are indicated and it is observed the strong decrease of M_S for sample 27Mn12Cr, which results from combined phenomena: the introduction of dislocations during FCC-HCP thermal cycling and the FCC stabilization due to the para-antiferromagnetic transition.
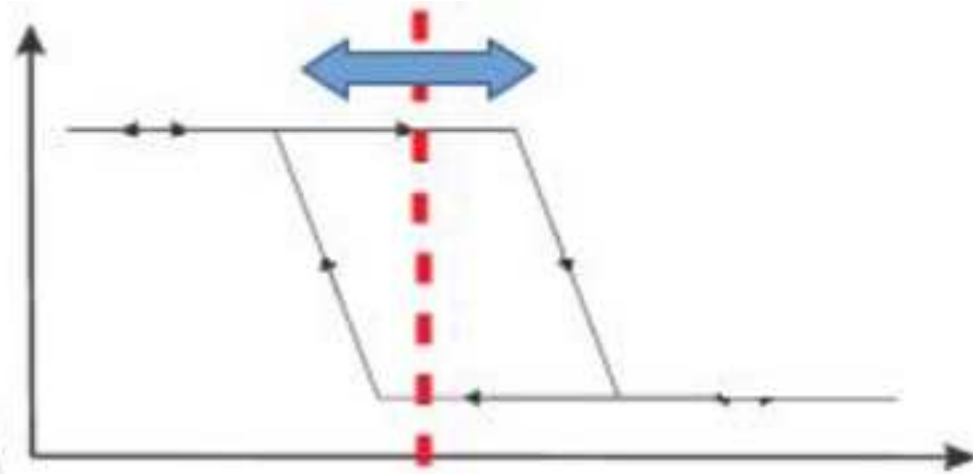
- Grain size reduction
- FCC antiferro ordering
- FCC Plastic deformation
- Thermal cycling
- Combined effects

Highlights:

- Several strategies to increase the FCC austenite stability in High-Mn steels have been presented
- For grain size of 2 μm the suppression of the BCC martensite was found in binary alloys
- Néel temperatures show some discrepancies with models presented in the literature
- The effect of grain size on the FCC-HCP transition was analyzed
- Thermal cycling combined with magnetic ordering can be used to stabilize the austenite
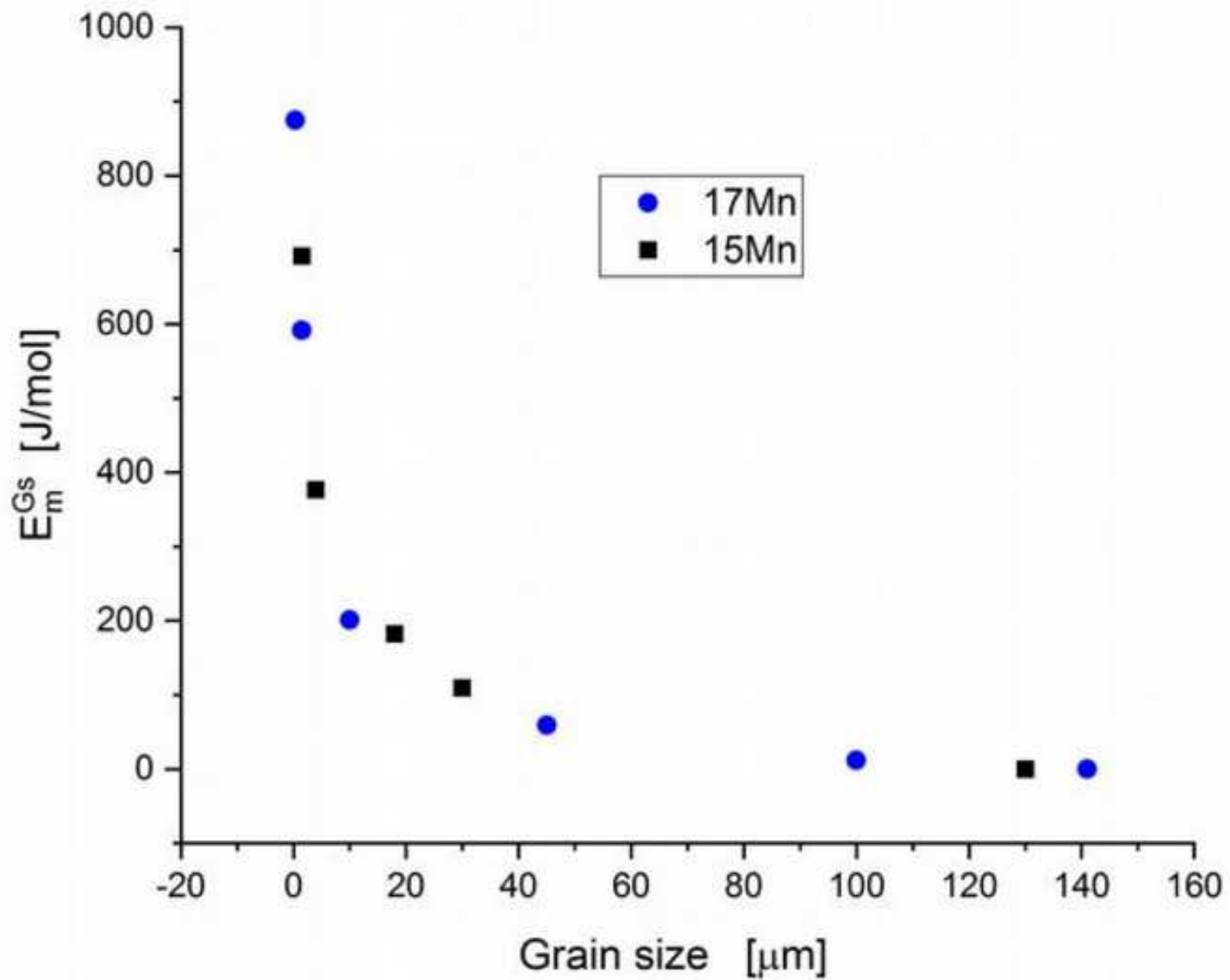
Figure 1
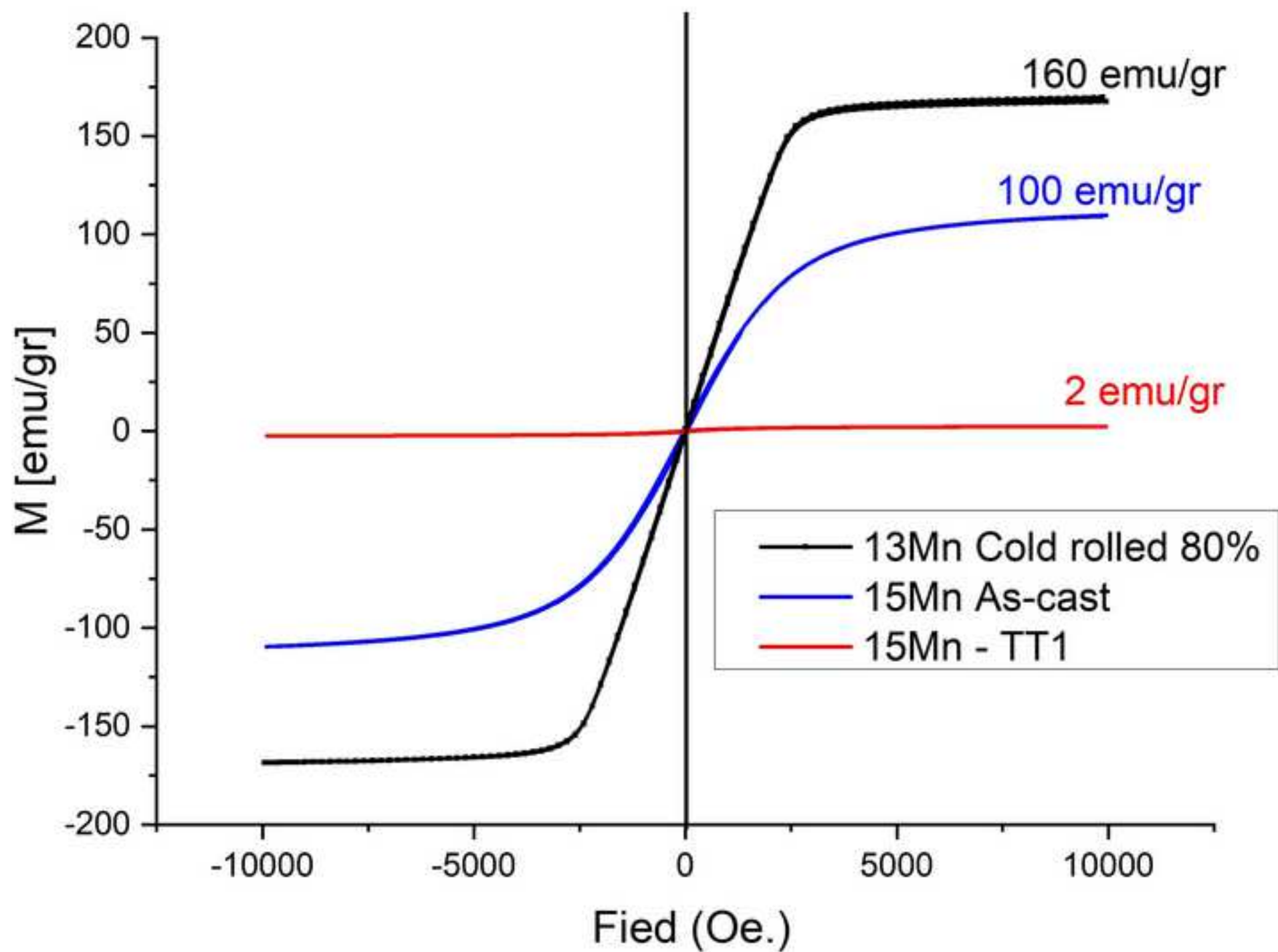
Figure 2
Click here to download high resolution image
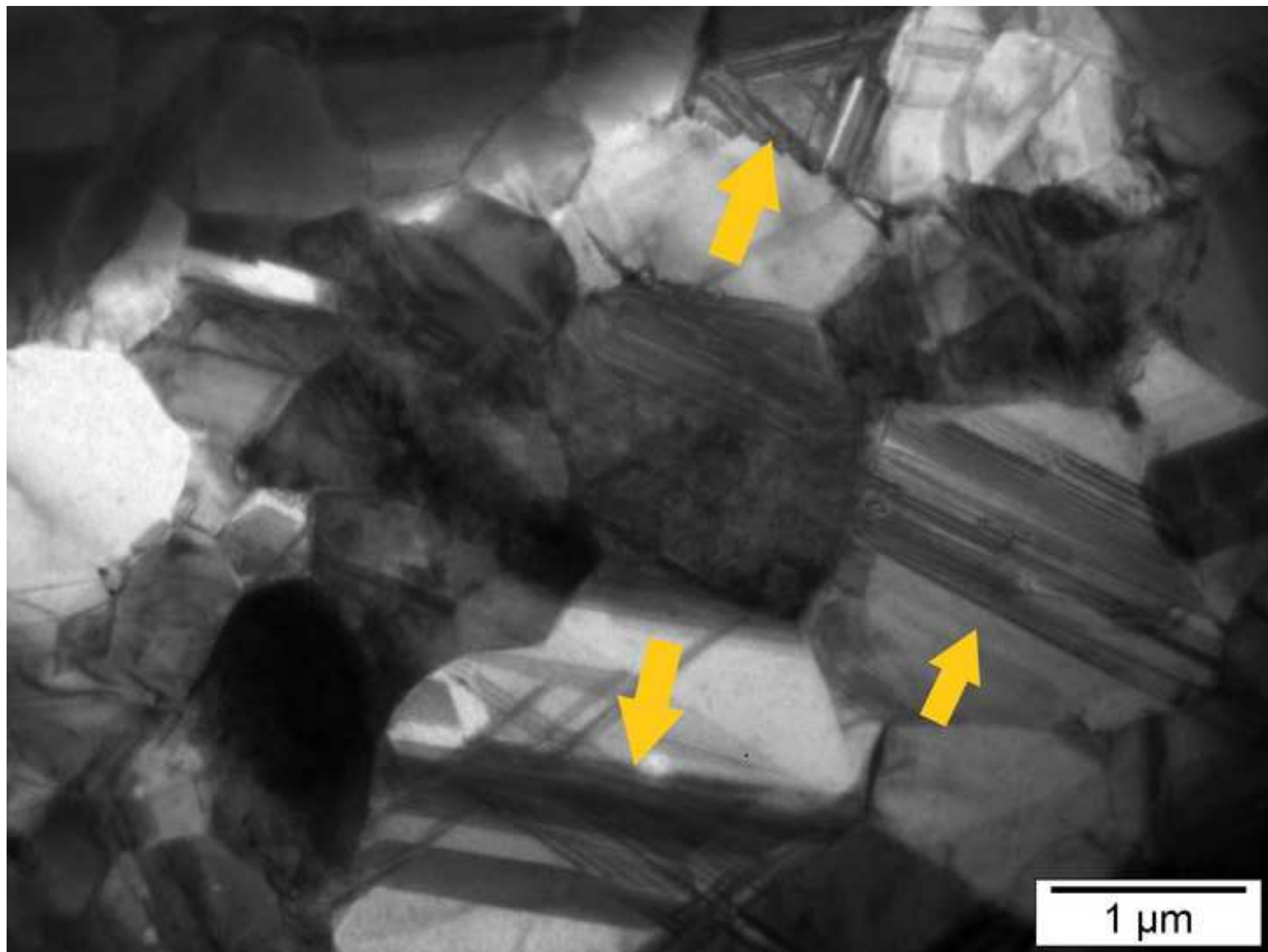
Figure 3
Click here to download high resolution image
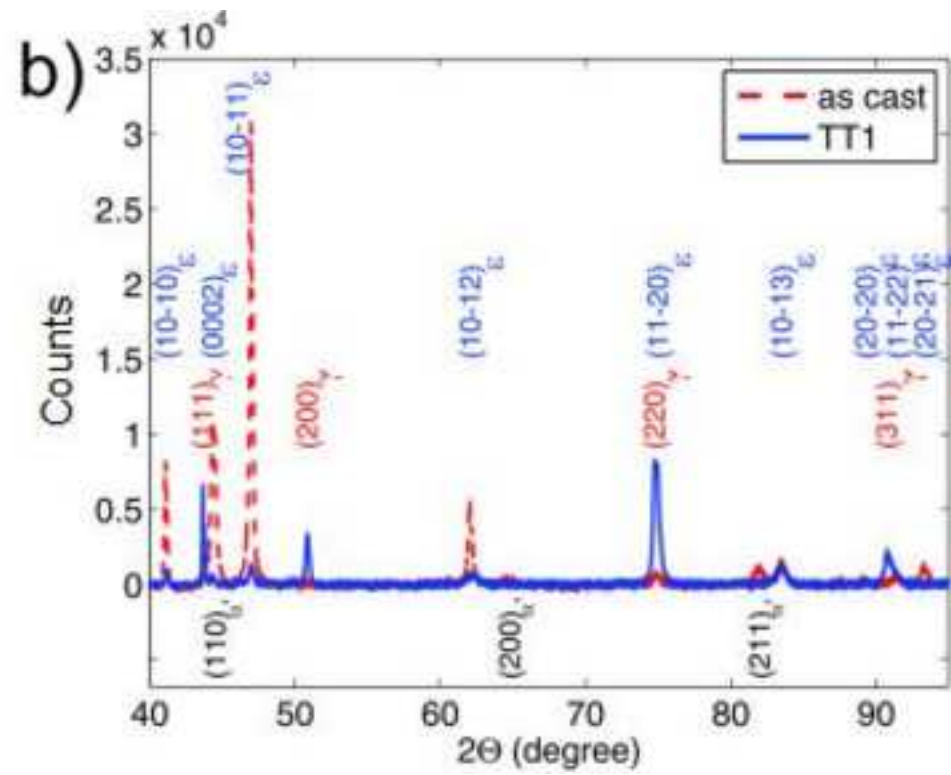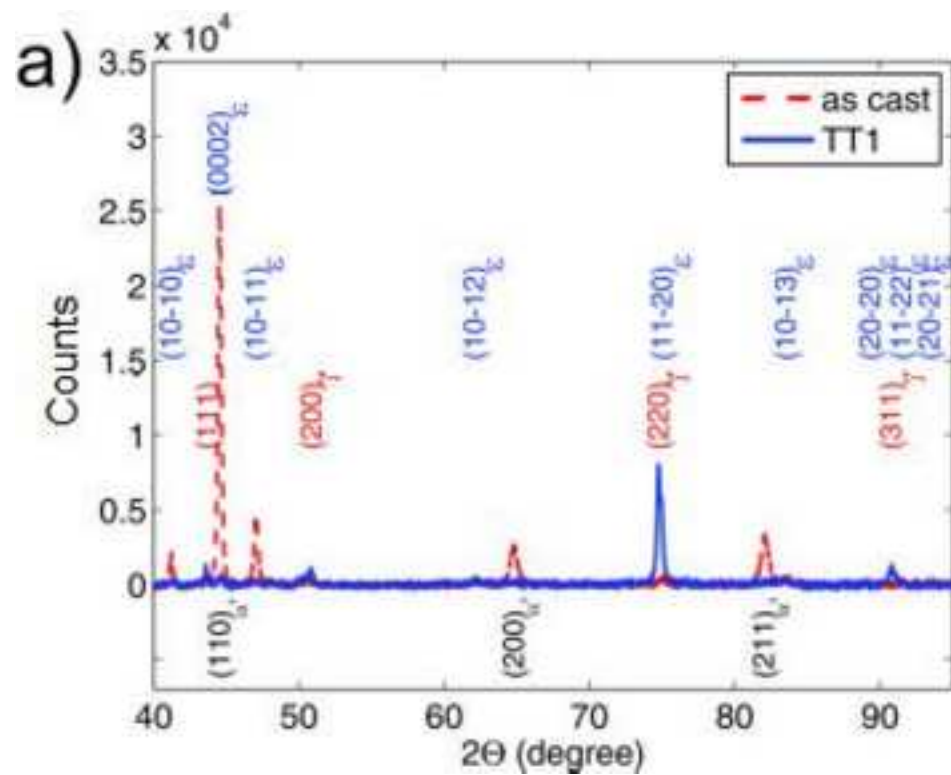
Figure 4
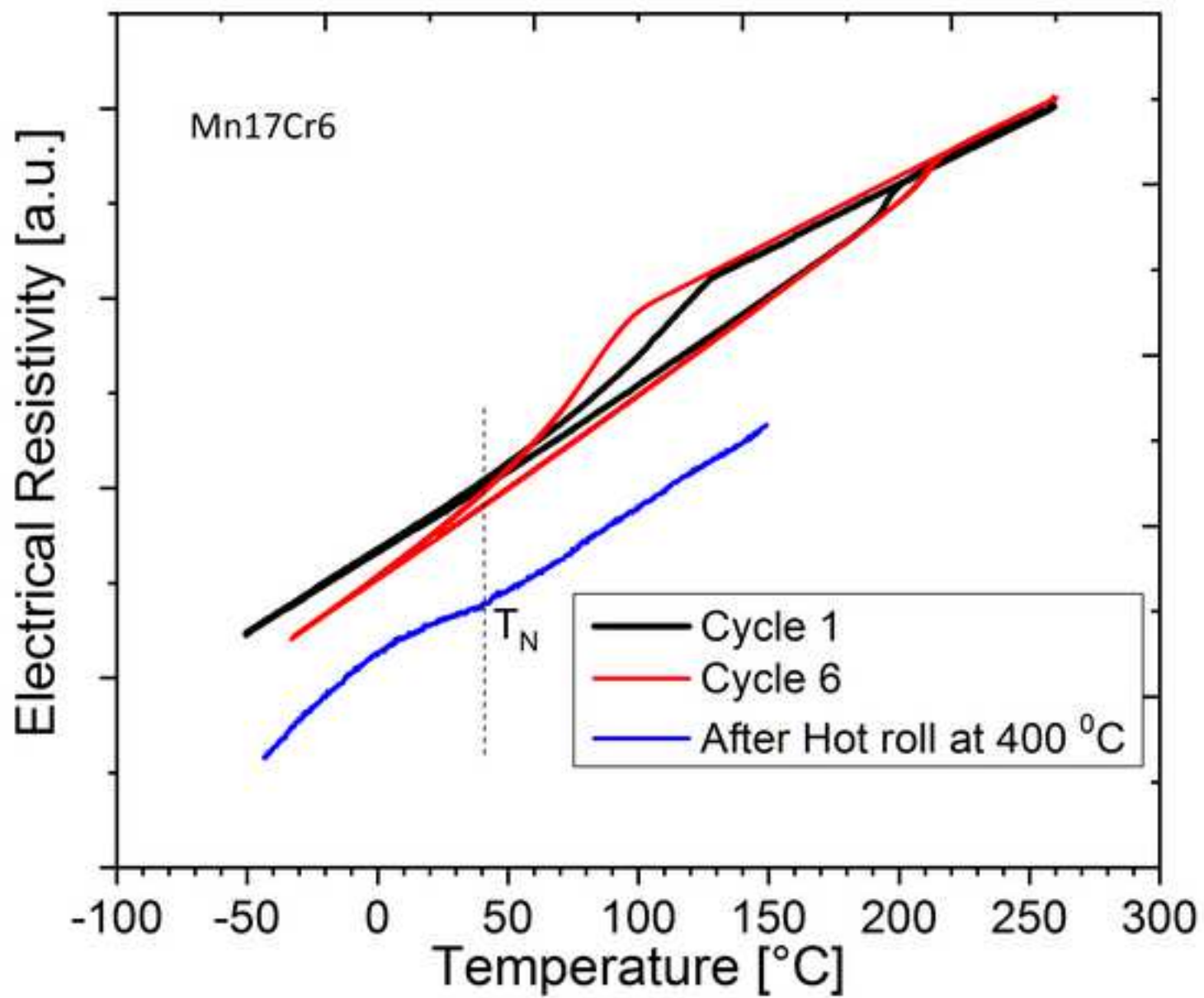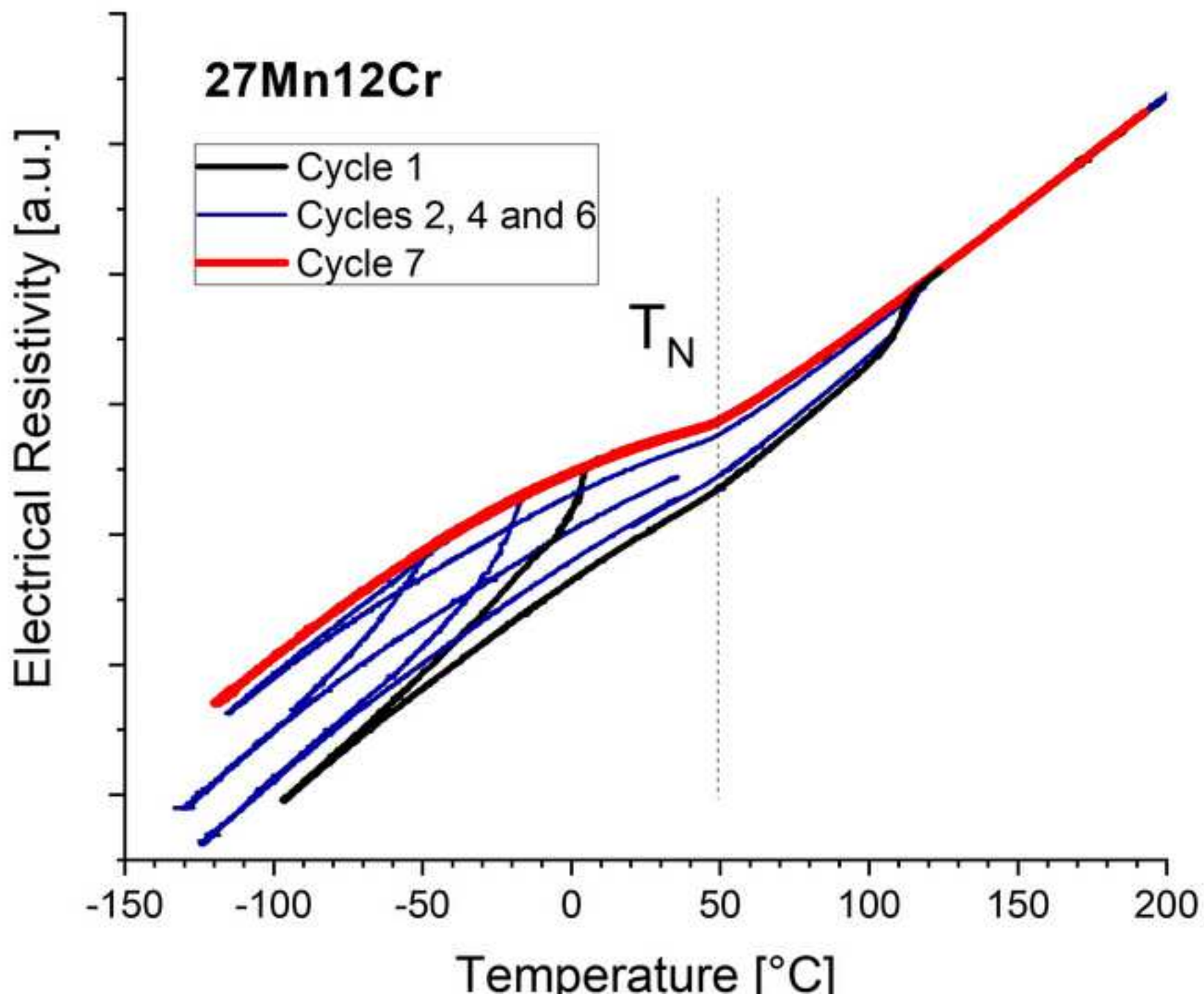**Click here to download high resolution image**
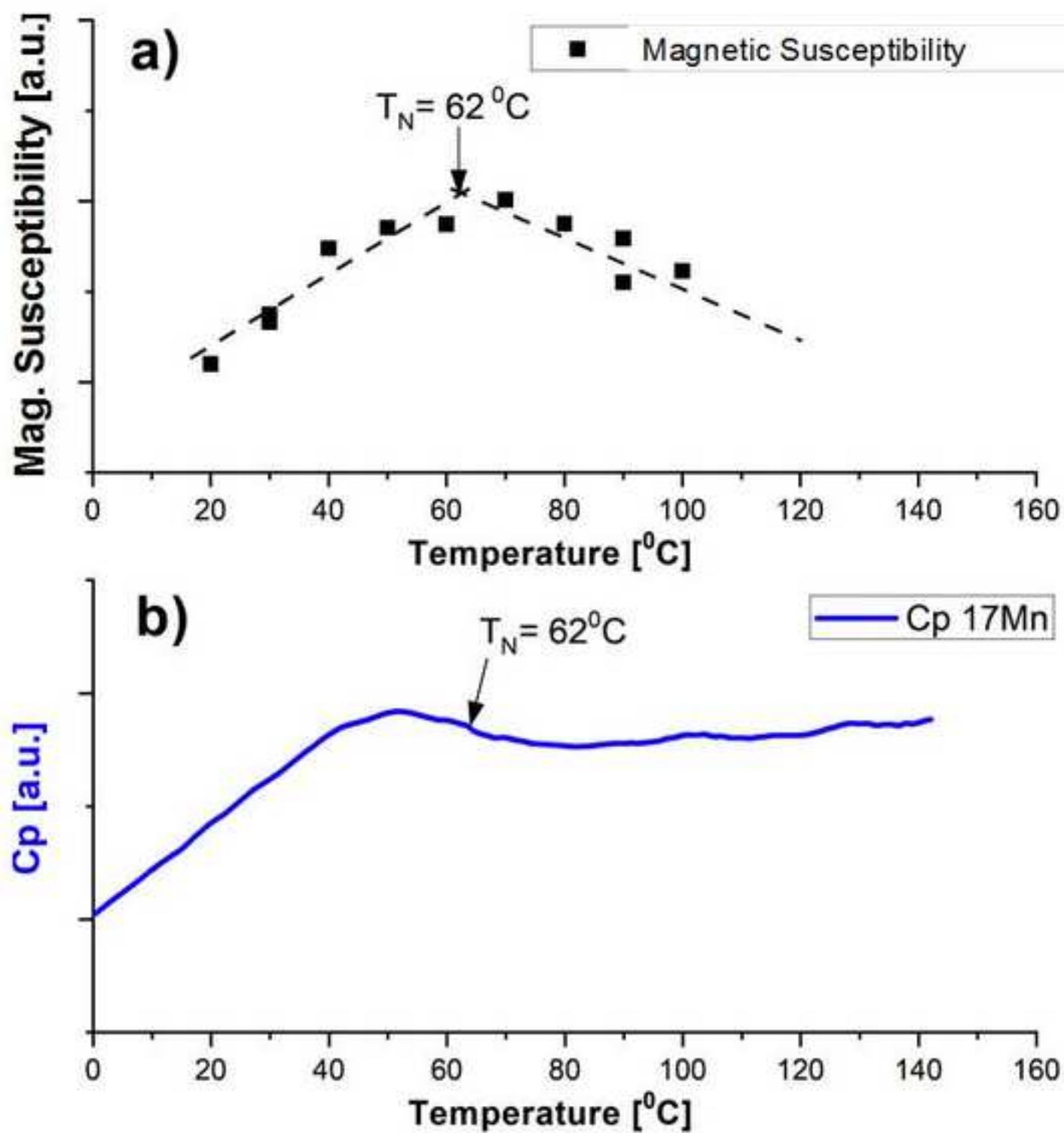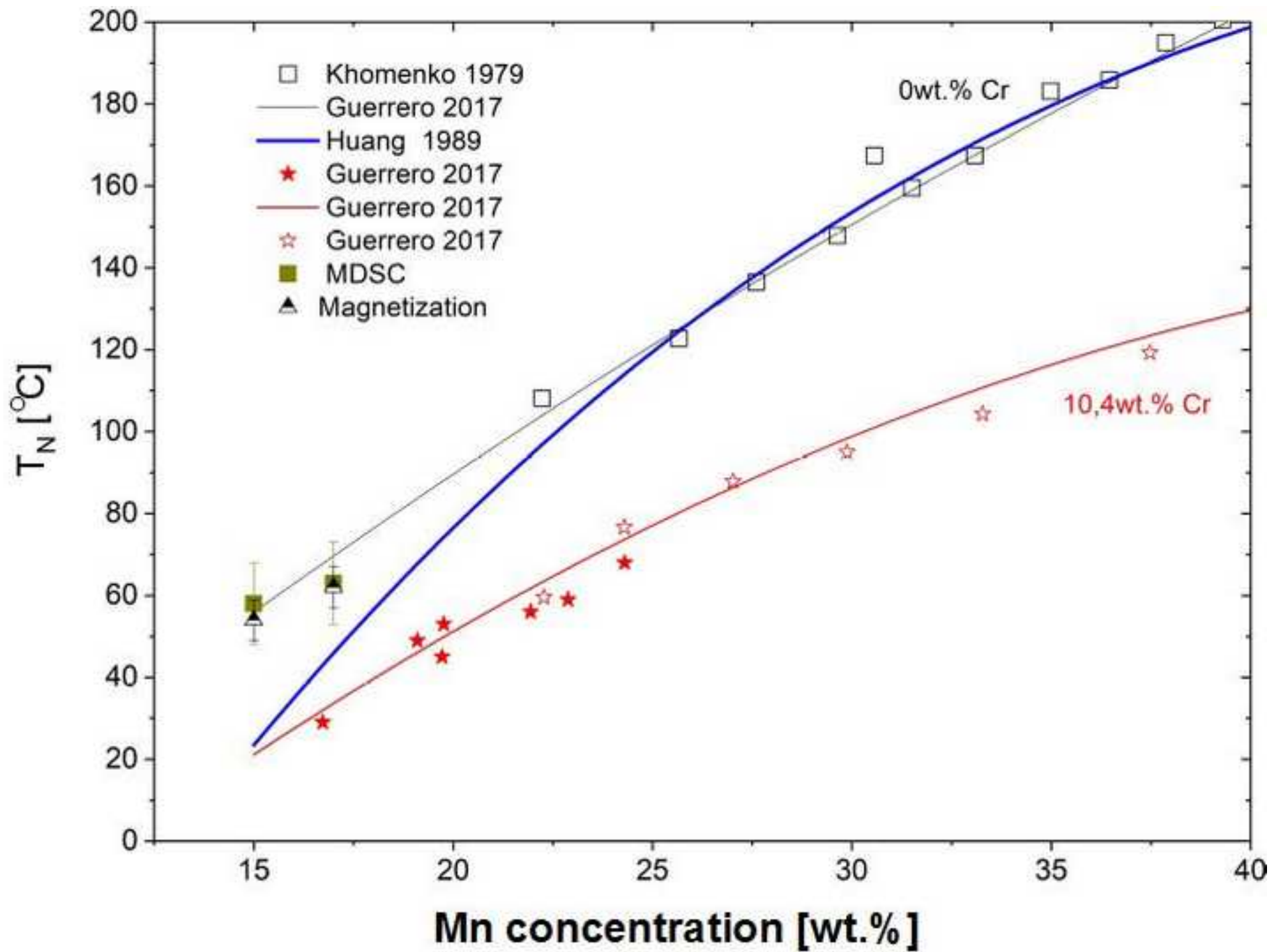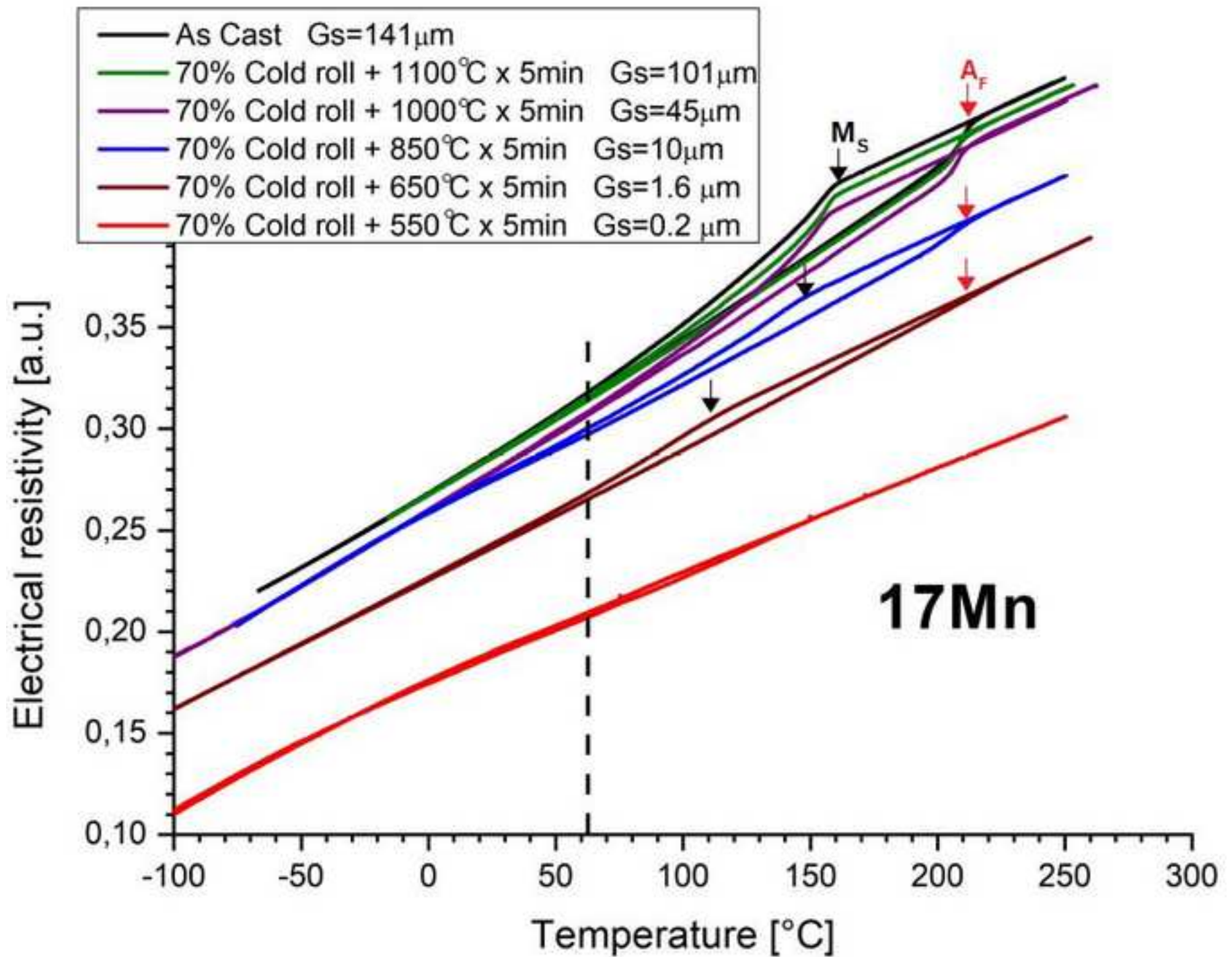
Figure 4

Figure 7
Click here to download high resolution image
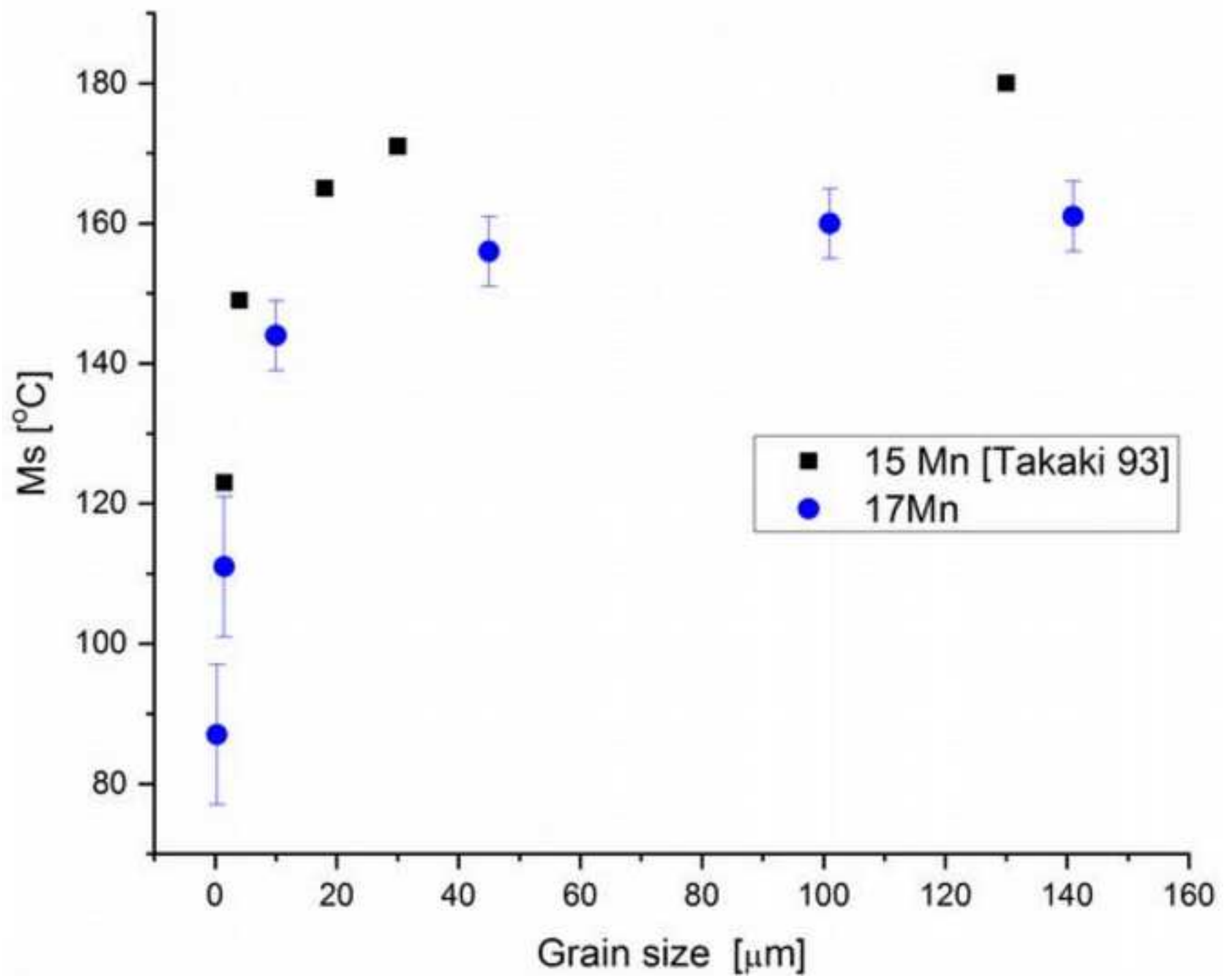
Figure 7

Figure 8
Click here to download high resolution image

Figure 10
Click here to download high resolution image

Figure 10

Figure 11
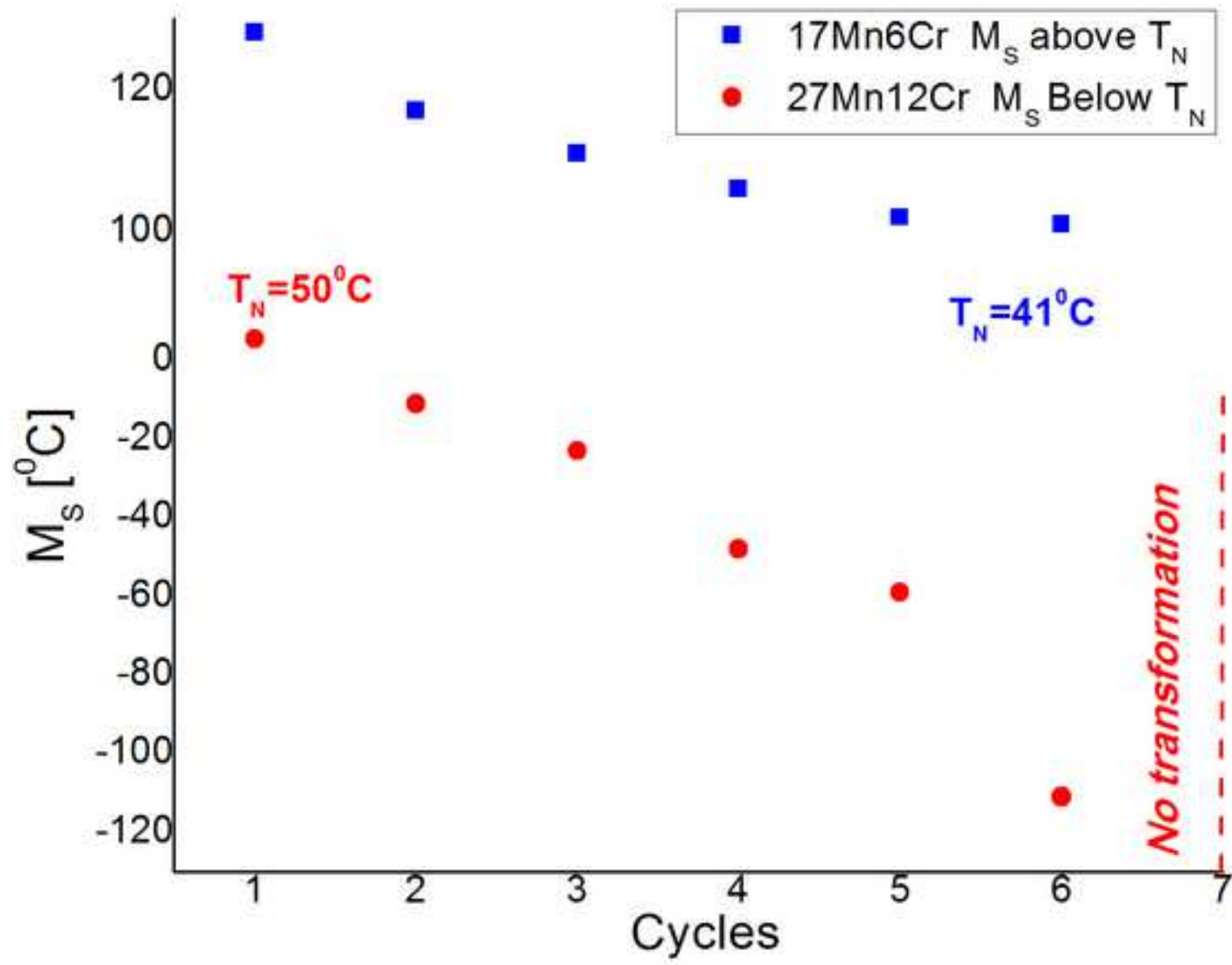
Credit author statement:

All authors participated on: Conceptualization, Methodology, Investigation, Data Curation and Writing the paper.

*Declaration of Interest Statement

Declaration of interests

☒ The authors declare that they have no known competing financial interests or personal relationships that could have appeared to influence the work reported in this paper.

☐The authors declare the following financial interests/personal relationships which may be considered as potential competing interests: